International Journal of Heat and Fluid Flow 116 (2025) 109933

Contents lists available at ScienceDirect

International Journal of Heat and Fluid Flow

journal homepage: www.elsevier.com/locate/ijhff

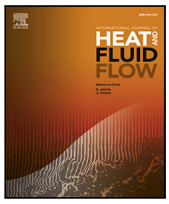

Enhancement of wall-bounded turbulence by solid particles under gravity

Yutaro Motoori *, Susumu Goto

Graduate School of Engineering Science, The University of Osaka, 1-3 Machikaneyama, Toyonaka, Osaka, 560-8531, Japan

ARTICLE INFO

Keywords:
Turbulence modulation
Solid particles
Turbulent channel flow

ABSTRACT

When we add solid particles to turbulent flow, the turbulence can be either attenuated or enhanced. Both phenomena are caused by the wakes of particles. More specifically, turbulence attenuation is due to the additional energy dissipation in the wakes, while turbulence enhancement is due to the additional turbulent energy by the wakes. In the present study, we propose a scenario for turbulence modulation in terms of particle wakes and verify it using direct numerical simulation data of turbulent channel flow in the presence of gravity. We show that the total turbulent kinetic energy is enhanced when the relative velocity becomes larger so that a significant turbulent energy is introduced locally by particle wakes. This does not happen in the absence of gravity.

1. Introduction

When we add solid particles to turbulent flow, even in a small volume fraction of particles, turbulent kinetic energy can be significantly attenuated or enhanced. In the past, experiments have played a primary role in elucidating the physical mechanism underlying turbulence modulation. The pioneering study of Gore and Crowe (1989) compiled experimental results (Serizawa et al., 1975; Maeda et al., 1980; Lee and Durst, 1982; Theofanous and Sullivan, 1982; Tsuji et al., 1984, e.g.) available at the time, demonstrating that turbulence intensity is attenuated when the particle diameter is approximately 0.1 times smaller than the integral length of turbulence, whereas larger particles tend to enhance turbulence. Regarding turbulence attenuation due to small particles, the observation is consistent with the results of subsequent experiments (Kulick et al., 1994; Rogers and Eaton, 1991; Fessler and Eaton, 1999; Kussin and Sommerfeld, 2002; Yang and Shy, 2005) and numerical simulations (Ferrante and Elghobashi, 2003; Ten Cate et al., 2004; Vreman, 2007; Zhao et al., 2010; Abdelsamie and Lee, 2012; Zhao et al., 2013; Li et al., 2016; Liu et al., 2017; Mortimer et al., 2019; Oka and Goto, 2022; Peng et al., 2023). Afterwards, other criteria were proposed, such as the particle Reynolds number (Hetsroni, 1989), the product of the relative velocity and particle diameter (Hosokawa and Tomiyama, 2004), the Stokes number (Righetti and Romano, 2004) and the particle moment number (Tanaka and Eaton, 2008). Although these studies accumulated a significant body of knowledge for describing turbulence enhancement and attenuation, a definitive conclusion has not yet been reached.

Meanwhile, thanks to direct numerical simulations (DNS) of turbulence interacting with finite-size particles, great progress has been made in understanding turbulence attenuation due to small particles. One of the most important observations, shown by many studies (Ten Cate et al., 2004; Burton and Eaton, 2005; Lucci et al., 2010; Yeo et al., 2010; Bellani et al., 2012; Wang et al., 2014; Schneiders et al., 2017; Uhlmann and Chouippe, 2017; Oka and Goto, 2022; Shen et al., 2022; Peng et al., 2023; Balachandar et al., 2024), is that the additional energy dissipation rate ϵ_p due to particles is key to describing turbulence attenuation. More specifically, when a large slip velocity is produced between particles and the surrounding fluid, the energy dissipation rate ϵ_p is added around the particles. This additional ϵ_p bypasses a part of the energy flux in turbulence, leading to the attenuation of turbulent kinetic energy generated through the energy cascade. On the basis of this physical mechanism, Oka and Goto (2022) derived a formula to estimate the attenuation rate of turbulent kinetic energy and verified it using their DNS results of turbulence in a periodic box. Similarly, Balachandar et al. (2024) also proposed another formula to predict the attenuation rate on the basis of a similar picture. Recently, we (Motoori and Goto, 2025) also demonstrated that ϵ_p plays a crucial role in turbulence attenuation in wall-bounded turbulence, where the energy production rate due to the mean flow is reduced by the amount of ϵ_p. Incidentally, the picture based on ϵ_p is consistent with the result of Gore and Crowe (1989) since ϵ_p becomes larger for smaller particles if the volume fraction is constant (Oka and Goto, 2022; Motoori and Goto, 2025). However, most of these studies focused on turbulence

* Corresponding author.
E-mail addresses: y.motoori.es@osaka-u.ac.jp (Y. Motoori), s.goto.es@osaka-u.ac.jp (S. Goto).

https://doi.org/10.1016/j.ijheatfluidflow.2025.109933
Received 15 January 2025; Received in revised form 30 April 2025; Accepted 3 June 2025
Available online 27 June 2025

modulation by small particles without the gravitational effects, where we rarely observe turbulence enhancement; see the studies (Dritselis and Vlachos, 2008; Lee and Lee, 2015; Fornari et al., 2016; Yu et al., 2017; Muramulla et al., 2020; Costa et al., 2021; Shen et al., 2024) in addition to those cited above. Besides, turbulence enhancement can locally occur in the near-wall regions even in the absence of gravity (Peng et al., 2019).

Recently, Yu et al. (2021) and Xia et al. (2021) examined turbulence modulation in a wide parameter space, where both turbulence enhancement and attenuation occur, by conducting DNS of turbulent channel flow under gravity (parallel to the streamwise direction) laden with particles. Yu et al. (2021) proposed a criterion to describe whether turbulent kinetic energy is enhanced or attenuated by fitting the obtained data. This criterion is consistent with not only their data but also experimental results used by Gore and Crowe (1989), recent experiments (Hosokawa and Tomiyama, 2004; Shokri et al., 2017; Mena and Curtis, 2020) and DNS (Uhlmann, 2008). Although many studies also observed turbulence enhancement in the presence of gravity (Kajishima et al., 2001; Uhlmann, 2008), the relevance of Yu et al. (2021)'s criterion to the physical phenomena of turbulence modulation remains unclear.

In the present study, we propose a scenario describing the physical mechanism of turbulence modulation by solid particles. On the basis of this scenario, we introduce an indicator over which turbulence is enhanced (Section 2). We then conduct DNS of turbulent channel flow under gravity laden with finite-size particles (Section 3). Using the obtained data, and the DNS results of Yu et al. (2021) and Motoori and Goto (2025), we verify the proposed scenario over a wide parameter space (Section 4). In this scenario, the slip velocity between particles and fluid plays a key role in both the enhancement and attenuation of turbulence; however, its role differs between these two phenomena. Through this article, we emphasise that this perspective is important for elucidating turbulence modulation by particles.

2. Scenario for turbulence modulation

For the dilute volume fraction Λ_p of particles, e.g. $\Lambda_p \lesssim \mathcal{O}(10^{-2})$, we describe below a scenario of turbulence modulation by the addition of particles. The scenario is not inconsistent with observations for turbulence enhancement (Uhlmann, 2008; Brandt and Coletti, 2022) and attenuation (Oka and Goto, 2022; Balachandar et al., 2024; Motoori and Goto, 2025) reported in previous studies.

Turbulent kinetic energy is injected by the external force and/or the mean flow in single-phase flow. However, when adding particles, the additional turbulent energy is introduced by the particle wakes. Thus, the total turbulent kinetic energy K is expressed as the summation of K_t, the energy generated without interactions with particles, and K_p, the energy added by the particle wakes: namely,

$$K = (1 - \Lambda_w)K_t + \Lambda_w K_p. \tag{1}$$

Here, Λ_w denotes the volume fraction of the particle wakes, being proportional to Λ_p if turbulence within the wake is fully developed. By dividing both sides of (1) by the turbulent kinetic energy $K_\times$ without the particle addition, where $\cdot_\times$ denotes the value in the single-phase flow, we obtain

$$\frac{K}{K_\times} = (1 - \Lambda_w)\frac{K_t}{K_\times} + \Lambda_w \frac{K_p}{K_\times}. \tag{2}$$

Therefore, whether turbulence is enhanced ($K/K_\times > 1$) or attenuated ($K/K_\times < 1$) depends on the relative contributions of K_t and K_p.

It is important to note that K_t decreases as a function of the relative velocity $|\Delta u|$ between particles and fluid, whereas K_p increases with $|\Delta u|$. We explain these trends as follows. The turbulent kinetic energy K_t, generated without interactions with particles, is determined by the turbulent energy flux ϵ_t ($\sim K_t^{3/2}/L$ with L being the integral length of turbulence). Then, the energy flux ϵ_t is reduced due to the additional energy dissipation rate ϵ_p, i.e. $\epsilon_t = \epsilon_\times - \epsilon_p$. Since ϵ_p is proportional to $|\Delta u|^3$,[1] K_t is a decreasing function of ϵ_p, and therefore of $|\Delta u|$.

In contrast, the turbulent energy K_p, locally added by particle wakes, is determined by the relative velocity as $K_p \approx |\Delta u|^2/2$. In other words, K_p is an increasing function of $|\Delta u|$. Therefore, a significant relative velocity leads to attenuation of K_t and enhancement of K_p. The modulation rate $K/K_\times$ of the total turbulent kinetic energy is determined by the competition between the attenuation of K_t and the enhancement of K_p.

In the present study, we focus on the case where turbulence is enhanced. For the condition $K/K_\times > 1$ to be satisfied, we need

$$\Lambda_w \frac{K_p}{K_\times} > 1 - (1 - \Lambda_w)\frac{K_t}{K_\times}. \tag{4}$$

For the dilute case ($1 - \Lambda_w \approx 1$), the right-hand side means the attenuation rate $1 - K_t/K_\times$ of the turbulence generated independently of particles. Thus, turbulence enhancement occurs as long as the additional turbulent energy $\Lambda_w K_p$ by the wakes is larger than this attenuation. In other words, even if K_t is significantly attenuated (i.e. $K_t \approx 0$), turbulence is enhanced when the condition

$$\sqrt{\Lambda_w}\,\frac{|\Delta u|}{u'_\times} \gtrsim 1 \tag{5}$$

is satisfied, where $u'_\times$ denotes the magnitude of the fluctuation velocity in the single-phase flow. This indicates the sufficient condition for turbulence enhancement irrespective of the extent of K_t attenuation. In the rest of this article, we demonstrate that $\sqrt{\Lambda_w}\,|\Delta u|/u'_\times$ in (5) is a good indicator by analysing DNS data.

Note that (5) is not satisfied unless the gravitational effect is sufficiently large. This is because, in the absence of gravity, the relative velocity $|\Delta u|$ cannot become significantly larger than the characteristic turbulent velocity $u'_\times$, even if the velocity relaxation time of particles is long enough [see Figs. 3a and 3c in Oka and Goto (2022) and the theoretical argument in Balachandar (2009)]. In other words, without the gravity, $|\Delta u|$ is at most comparable to $u'_\times$, i.e. $|\Delta u| \lesssim u'_\times$, and therefore the condition (5) cannot be satisfied in a dilute regime. In contrast, (5) can hold under gravity. Incidentally, in the presence of extremely large gravity, since turbulence generated by the particle wakes dominates, the flow differs substantially from the flow without particles. Since the comparison with the unladen flow is no longer meaningful in such a case, we restrict ourselves within the case with moderate gravity.

In summary, (5) is the sufficient condition for turbulence enhancement regardless of attenuation rate of K_t. Since this condition cannot hold without gravity, we conduct DNS that incorporate the gravitational effect in order to verify (5).

3. Methods

3.1. Direct numerical simulations

In this subsection, we describe the numerical method for the present DNS of turbulent channel flow in the presence of finite-size particles and gravity. We numerically simulate the flow field using the finite difference method, and the interaction between fluid and particles is expressed by the immersed boundary method by Breugem (2012), originally proposed by Uhlmann (2005). The flow obeys the Navier–Stokes equation,

$$\frac{\partial \boldsymbol{u}}{\partial t} + (\boldsymbol{u}\cdot\boldsymbol{\nabla})\boldsymbol{u} = -\frac{1}{\rho_f}\boldsymbol{\nabla} p + \nu\nabla^2\boldsymbol{u} + f_{pg}\boldsymbol{e}_x + \boldsymbol{f}_{IBM}, \tag{6}$$

[1] The energy dissipation rate around particles is estimated by

$$\epsilon_p \sim \Lambda_p \frac{|\Delta u|^3}{D} \tag{3}$$

through the dimensional analysis.

Table 1
Particle parameters.

D^+	D/h	ρ_p/ρ_f	St_h	N_p	Λ_p	u_g/u_τ
32	0.18	2	0.16	178	0.0082	0
32	0.18	2	0.16	178	0.0082	2
32	0.18	2	0.16	178	0.0082	4
32	0.18	2	0.16	178	0.0082	6
32	0.18	2	0.16	178	0.0082	8
32	0.18	128	10	178	0.0082	0
32	0.18	128	10	178	0.0082	2
32	0.18	128	10	178	0.0082	4
32	0.18	128	10	178	0.0082	6
32	0.18	128	10	178	0.0082	8
64	0.36	2	0.63	22	0.0082	0
64	0.36	2	0.63	22	0.0082	2
64	0.36	2	0.63	22	0.0082	4
64	0.36	2	0.63	22	0.0082	6
64	0.36	2	0.63	22	0.0082	8
64	0.36	128	40	22	0.0082	0
64	0.36	128	40	22	0.0082	2
64	0.36	128	40	22	0.0082	4
64	0.36	128	40	22	0.0082	6
64	0.36	128	40	22	0.0082	8
32	0.18	2	0.16	89	0.0041	0
32	0.18	2	0.16	89	0.0041	2
32	0.18	2	0.16	89	0.0041	4
32	0.18	2	0.16	89	0.0041	6
32	0.18	2	0.16	89	0.0041	8

and the continuity equation,

$$\boldsymbol{\nabla}\cdot\boldsymbol{u}=0. \tag{7}$$

Here, $\boldsymbol{u}(\boldsymbol{x},t)$ and $p(\boldsymbol{x},t)$ are the fluid velocity and pressure at position $\boldsymbol{x}$ and time t, respectively, ρ_f is the fluid mass density, $f_{pg}(t)$ is time-dependent force per unit mass due to the external pressure difference, $\boldsymbol{e}_x$ is the unit vector in the streamwise direction and $\boldsymbol{f}_{IBM}$ is the force per unit mass to satisfy the non-slip boundary condition on the surface of each particle. The driving force $f_{pg}(t)$ is imposed so that the flow rate keeps constant. The Reynolds number based on the spatial average velocity U_b is $Re_b = U_b h/\nu = 2873$, which corresponds to the friction Reynolds number $Re_\tau = u_\tau h/\nu = 180$ in the case without particles. Here, u_τ is the friction velocity (in the single-phase flow), h is the channel-half width and ν is the kinetic viscosity. The side lengths of the computational box are 8 h, 2 h and 4 h in the streamwise (x), wall-normal (y) and spanwise (z) directions, respectively. The grid width is set to $\Delta^+_{grid} = 2$ for all directions, where $\cdot^+$ denotes the quantity normalised by u_τ and ν.

Each particle with the velocity $\boldsymbol{u}_p(t) = \mathrm{d}\boldsymbol{x}_p/\mathrm{d}t$ and angular velocity $\boldsymbol{\omega}_p(t)$ is governed by the equations of motion for translation,

$$\rho_p V_p \frac{\mathrm{d}\boldsymbol{u}_p}{\mathrm{d}t} = \oint_{\partial V_p} \mathbf{T}\cdot\boldsymbol{n}\,\mathrm{d}S + \rho_f V_p f_{pg}\boldsymbol{e}_x + \rho_p V_p g\boldsymbol{e}_x + \boldsymbol{F}^{\leftrightarrow p}, \tag{8}$$

and rotation,

$$I_p \frac{\mathrm{d}\boldsymbol{\omega}_p}{\mathrm{d}t} = \oint_{\partial V_p} \boldsymbol{r}\times(\mathbf{T}\cdot\boldsymbol{n})\,\mathrm{d}S + \boldsymbol{T}^{\leftrightarrow p}, \tag{9}$$

of a rigid sphere. Here, ρ_p, V_p and I_p are the mass density, volume and moment of inertia of a spherical particle, respectively. In the right-hand side of (8) and (9), $\mathbf{T}$ is the stress tensor for a Newtonian fluid, $\boldsymbol{n}$ is the outward-pointing normal vector on the surface ∂V_p of the particle, g is the magnitude of the gravitational acceleration, $\boldsymbol{r}$ is the position vector relative to the particle centre, and $\boldsymbol{F}^{\leftrightarrow p}$ and $\boldsymbol{T}^{\leftrightarrow p}$ are the force and torque acting on the particle due to collisions with other particles and solid walls, respectively. We evaluate $\mathbf{T}$ by using the immersed boundary method (Breugem, 2012), and evaluate $\boldsymbol{F}^{\leftrightarrow p}$ and $\boldsymbol{T}^{\leftrightarrow p}$ using the elastic contact model (Glowinski et al., 2001). In addition, we set g to be positive, meaning that particles settle in the same direction as the flow.

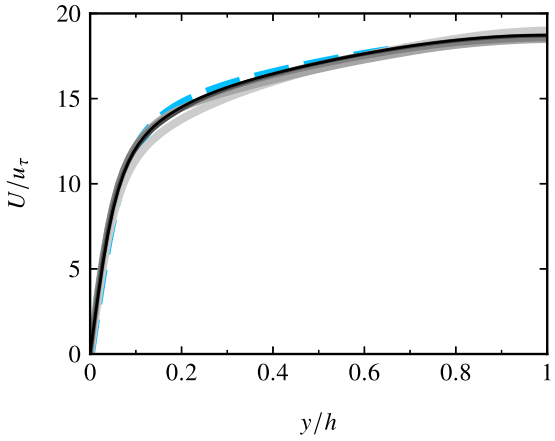

Fig. 1. Wall-normal profiles of the mean streamwise velocity U. The five lines show the results for the same diameter $D/h = 0.18$ and mass density $\rho_p/\rho_f = 2$ but different values of the settling velocity u_g/u_τ. From thinner (and darker) to thicker (and lighter), $u_g/u_\tau = 0$, 2, 4, 6 and 8. The blue dashed line shows the result for the single-phase flow.

The numerical method is the same as in Breugem (2012) and Motoori and Goto (2025) except for the time integration, for which we employ the second-order Crank–Nicolson method for the viscous term of the fluid and second-order Adams–Bashforth method for the others. The time interval is set to $\Delta t^+ = 0.02$ and 0.01 for $\rho_p/\rho_f = 2$ and 128, respectively.

3.2. Parameters

The particles are characterised by four parameters related to the particle diameter D, mass density ratio ρ_p/ρ_f between particles and fluid, number N_p of the added particles and magnitude g of the gravitational acceleration. In the present study, we change these four parameters to simulate 25 different types of particles, as listed in Table 1. For 20 of these particles, we fix the particle volume fraction Λ_p ($= N_p V_p/(64h^3)$) at = 0.0082. The particle diameters are $D^+ = 32$ and 64 (i.e. $D/h = 0.18$ and 0.36), corresponding to $D/\Delta_{grid} = 16$ and 32. The mass density ratios are $\rho_p/\rho_f = 2$ and 128, and for these particles, we change u_g. Here,

$$u_g = \sqrt{\frac{4(\rho_p/\rho_f - 1)Dg}{3}} \tag{10}$$

is characteristic settling velocity of particles due to gravity, estimated by assuming the drag coefficient $C_D = 1$ for the force balance $(\rho_p - \rho_f)gV_p = C_D\rho_f u_g^2 (D/2)^2\pi/2$ in the quiescent fluid. The direction of u_g aligns with the fluid streamwise direction, that is, the vertical downward channel flow. In Appendix A, we show results for the upward channel flow, and there is no significant difference in the behaviour of turbulence modulation between the two flows. As shown at the rightmost column in Table 1, we systematically change u_g/u_τ to 0, 2, 4, 6 and 8. In wall-bounded turbulence, since the fluctuation velocity is comparable with u_τ for all y, u_g/u_τ represents the ratio of the particle settling velocity to the characteristic velocity of turbulence. Note that for the same diameter and mass density, u_g varies with g.

We also simulate the case with a smaller volume fraction, $\Lambda_p = 0.0041$, corresponding to 5 types of particles shown in Table 1 under the line. Here, we fix $D/h = 0.18$ and $\rho_p/\rho_f = 2$, while changing u_g/u_τ (= 0–8).

In Table 1, St_h ($= \tau_p/\tau_h$) denotes the Stokes number, defined as the ratio of the velocity relaxation time τ_p ($= \rho_p D^2/(18\rho_f\nu)$) to the turnover time τ_h ($= h/u_\tau$) of the largest vortices. When $St_h < 1$, particles can

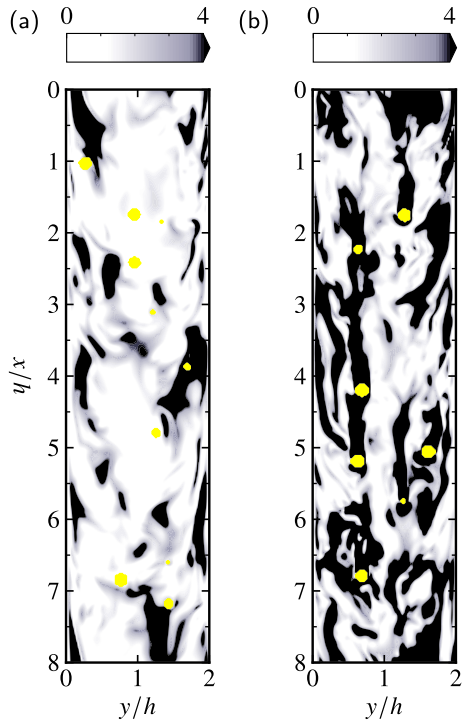

Fig. 2. Visualisations of turbulent kinetic energy $|\boldsymbol{u}'|^2/2$ on two-dimensional (y–x) plane for particles with the same diameter ($D/h = 0.18$), mass density ($\rho_p/\rho_f = 2$) and volume fraction ($\Lambda_p = 0.0082$) but different values of the settling velocity (a) $u_g/u_\tau = 0$ and (b) 8. Yellow circles are cross sections of the particles.

follow the swirling motion of the largest vortices ($\sim h$); otherwise, they cannot follow the swirls. For the case with $\rho_p/\rho_f = 128$, since $St_h \gg 1$ (see the fourth column in Table 1), the particles cannot follow the largest vortices.

Before showing results regarding the modulation of turbulent kinetic energy, we show in Fig. 1 the wall-normal profiles of the mean streamwise velocity $U(y)$ ($= \overline{u}$). Here, $\overline{\cdot}$ denotes the average in the homogeneous directions and over time in the statistically steady state.[2] The results shown in Fig. 1 are for the same diameter ($D/h = 0.18$) and mass density ($\rho_p/\rho_f = 2$) but different values of the settling velocity u_g/u_τ (thicker lighter lines represent larger u_g/u_τ). The blue dashed line shows the result for the single-phase flow. We can see that the mean velocity profiles approximately overlap irrespective of u_g/u_τ. It is also worth mentioning that the gradients of the mean velocity on the wall, and therefore the friction Reynolds numbers are not significantly altered for the examined parameters.[3] Incidentally, to validate DNS results, we confirmed in our previous study (Motoori and Goto, 2025) that our DNS reproduces the result of Yu et al. (2021). Moreover, we have also confirmed that even in the case with the largest gravity (i.e. $u_g/u_\tau = 8$), the wall-normal profile of turbulent kinetic energy K agrees well with that obtained using the finer resolution $\Delta^+_{grid} = 1.5$, with the error within the standard deviation of K. In the following, we investigate how turbulence is modulated.

[2] More specifically, we take the temporal average with a time interval $t/\tau_h = 1.1$ and 0.56 over the period $t/\tau_h = 6.6$–33 and 3.3–17 for $\rho_p/\rho_f = 2$ and 128, respectively. Here, $t = 0$ denotes the time when particles are added. We have confirmed that the turbulent kinetic energy becomes statistically steady after the initial transient.

[3] The values of the friction Reynolds number are 180–210.

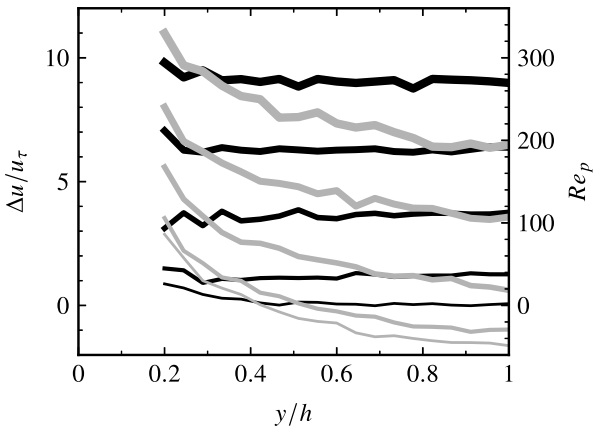

Fig. 3. Wall-normal profiles of the mean streamwise relative velocity Δu for $D/h = 0.18$ and $\rho_p/\rho_f = 2$ (black) and 128 (grey). The five lines show, from thinner to thicker, $u_g/u_\tau = 0$, 2, 4, 6 and 8. The right vertical axis indicates the particle Reynolds number Re_p ($= \Delta u D/\nu$).

4. Results

We first show results for $\Lambda_p = 0.0082$ in Sections 4.1–4.3. In Section 4.4, we also use the data for $\Lambda_p = 0.0041$ and DNS results by Yu et al. (2021) and Motoori and Goto (2025).

4.1. Visualisation

We visualise in Fig. 2 the spatial distributions of turbulent kinetic energy $|\boldsymbol{u}'|^2/2$ on y–x plane, where $\boldsymbol{u}' = \boldsymbol{u} - U\boldsymbol{e}_x$. The panels show results for the same diameter ($D/h = 0.18$) and mass density ($\rho_p/\rho_f = 2$) but different values of the settling velocity (a) $u_g/u_\tau = 0$ and (b) 8. Yellow regions are the cross sections of the particles. The directions of the flow and settling of particles are downward of the figure. In panel (a), we see that turbulent kinetic energy (shown by darker colour) is distributed independently of particles; whereas in (b), turbulent energy is prominent behind particles. This implies that significant turbulent energy K_p is added by the particle wakes when $u_g \gtrsim u_\tau$. This additional K_p leads to the enhancement of the total turbulent kinetic energy, as quantitatively shown below. Incidentally, particles distribute almost homogeneously (Appendix B). Hence, the effect of the particle accumulation on turbulence modulation is not significant for the examined parameters.

4.2. Relative velocity

Before showing results for turbulent kinetic energy, we first look at the parameter dependence of the relative velocity. Fig. 3 shows the wall-normal profiles of the mean streamwise relative velocity Δu for $D/h = 0.18$. Here, we define the mean relative velocity Δu ($= u_p - \langle u \rangle_p$) at each height as the particle velocity u_p minus the surrounding fluid velocity $\langle u \rangle_p$, where $\langle u \rangle_p$ is the average fluid velocity on the surface of a sphere with diameter $2D$ concentric with the particle (Kidanemariam et al., 2013; Uhlmann and Chouippe, 2017). Hence, when $\Delta u > 0$, the particle is faster than the surrounding fluid. The lines show, from thinner to thicker, the results for $u_g/u_\tau = 0$, 2, 4, 6 and 8. We see that for larger u_g, the relative velocity becomes larger at all distances y from the wall. This implies that the relative velocity is determined by the settling velocity u_g (if $u_g \gtrsim u_\tau$). More precisely, for heavy particles with large St_h (grey lines), the relative velocity depends on y. This is because particles with $St_h \gtrsim 1$ cannot follow turbulent eddies at any y, and therefore the velocity difference tends to be larger in the near-wall region where the fluid velocity is slower. Chouippe et al. (2023)

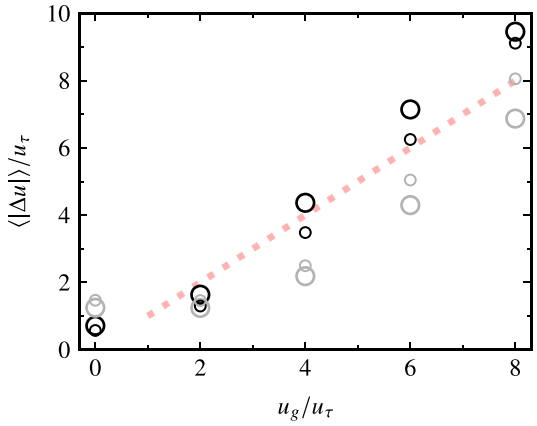

Fig. 4. Spatial average $\langle|\Delta u|\rangle$ of relative velocity as a function of the settling velocity u_g/u_τ of particles. The symbols show the results for $D/h = 0.18$ (smaller circles) and 0.36 (larger ones), and $\rho_p/\rho_f = 2$ (black) and 128 (grey). The red dotted line indicates $\langle|\Delta u|\rangle = u_g$.

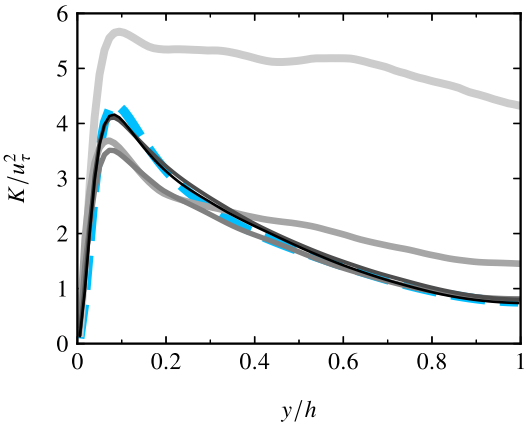

Fig. 5. Wall-normal profiles of the mean turbulent kinetic energy K for $D/h = 0.18$ and $\rho_p/\rho_f = 2$. The five lines show, from the thinner (and darker) to thicker (and lighter), $u_g/u_\tau = 0$, 2, 4, 6 and 8. The blue dashed lines shows the result for the single-phase flow.

summarised in section 6.4.1 of Subramaniam and Balachandar (2023) the behaviour of the relative velocity in vertical channel flow, and our observation is consistent with their results.

Fig. 4 shows the spatial average $\langle|\Delta u|\rangle$ of the absolute value of the relative velocity as a function of u_g. Both axes are normalised by u_τ. Here, $\langle\cdot\rangle$ denotes the average over the fluid region and time. The smaller and larger circles in the figure show $D/h = 0.18$ and 0.36, respectively, and black and grey ones show $\rho_p/\rho_f = 2$ and 128, respectively. We can observe that the circles lie approximately along the red dotted line, indicating that the average of the relative velocity is approximately u_g (when $u_g \gtrsim u_\tau$), although there is a small dependence on St_h due to the inhomogeneity in the wall-normal direction (Fig. 3).

4.3. Turbulent kinetic energy

We are ready to discuss the turbulence modulation. We show in Fig. 5 the mean turbulent kinetic energy K as a function of the distance y from the wall. The five grey lines show the results for the constant D/h (= 0.18) and ρ_p/ρ_f (= 2) but different values of u_g/u_τ. The blue dashed line shows the turbulent kinetic energy $K_\times$ in the single-phase flow. The profiles for $u_g/u_\tau = 0$ (the thinnest black line) and 2 (the second thinnest one) are similar to that for the single-phase flow. This implies that turbulence modulation does not occur for these parameters. In contrast, for the cases with $u_g/u_\tau = 4$ and 6, turbulent kinetic energy is attenuated for $y/h \lesssim 0.3$; whereas for $u_g/u_\tau = 6$, turbulent energy increases for $y/h \gtrsim 0.3$, and for $u_g/u_\tau = 8$, it is significantly enhanced over the entire channel. In other words, as u_g increases from 0, turbulence first gets attenuated; however, when u_g further increases, turbulence is enhanced. This is consistent with the scenario described in Section 2, which is further discussed in detail below.

Let us first consider the case with small u_g; $u_g/u'_\times$ ($\approx u_g/u_\tau$) $\lesssim \mathcal{O}(1)$. For this case, the relative velocity $|\Delta u|$ is almost determined by St_h, and even if St_h is sufficiently large, the relative velocity takes the value of $\mathcal{O}(u'_\times)$ at most. Balachandar (2009), Oka and Goto (2022), Motoori and Goto (2025). Hence, since $|\Delta u|$ is approximately less than or equal to $u'_\times$, for a small volume fraction of particles, the condition (5) does not hold. Therefore, the addition of turbulent kinetic energy by the particle wakes is not significant. Moreover, for this parameter (large diameter $D/h = 0.18$ and small Stokes number $St_h = 0.16$) shown in Fig. 5, since the energy dissipation rate ϵ_p due to particles is also small, the turbulent energy K_t is not significantly attenuated; consequently, the total turbulent energy K is not substantially modulated (see $u_g/u_\tau = 0$ and 2 in Fig. 5).

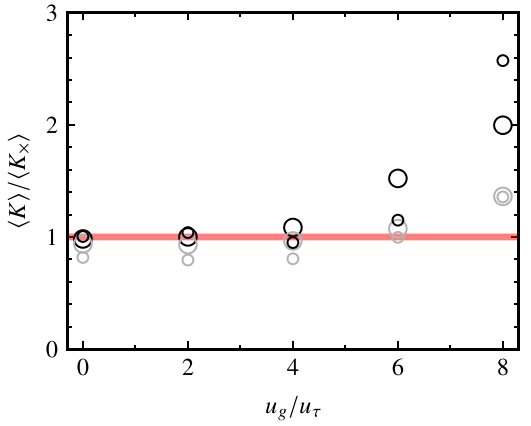

Fig. 6. Ratio of the spatial average of turbulent kinetic energy $\langle K\rangle$ to that $\langle K_\times\rangle$ for the single-phase flow as a function of the settling velocity u_g/u_τ of particles. The symbols show the results for $D/h = 0.18$ (smaller circles) and 0.36 (larger ones), and $\rho_p/\rho_f = 2$ (black) and 128 (grey). The red horizontal line shows $\langle K\rangle/\langle K_\times\rangle = 1$.

For moderately larger values of u_g/u_τ ($\gtrsim \mathcal{O}(1)$), although the relative velocity is slightly dependent on y and St_h, the average value is almost determined by the settling velocity u_g (Fig. 4). Such a non-negligible relative velocity $|\Delta u|$ results in an addition of energy dissipation rate ϵ_p in the wake behind particles, which leads to attenuation of the turbulent kinetic energy K_t (see $u_g/u_\tau = 4$ and 6 in Fig. 5). In addition, it is also important that when the relative velocity is large enough to satisfy the condition (5), the turbulent energy $\Lambda_w K_p$, locally added in the wakes, becomes significant (see the outer layer $y/h \gtrsim 0.3$ for $u_g/u_\tau = 6$ in Fig. 5). Therefore, K_t decreases, whereas K_p increases. If the attenuation rate of K_t and augmentation rate of K_p are comparable, the total turbulent energy K is not significantly modulated.[4]

[4] More precisely, looking at the case for $u_g/u_\tau = 6$ in Fig. 5, we see that turbulence enhancement occurs from the outer layer. We can explain this behaviour as follows. For this St_h (= 0.16), the relative velocity does not strongly depend on the distance from the wall (see the black lines in Fig. 3). In contrast, the fluid fluctuation velocity $u'_\times$ is slower in the outer than the inner

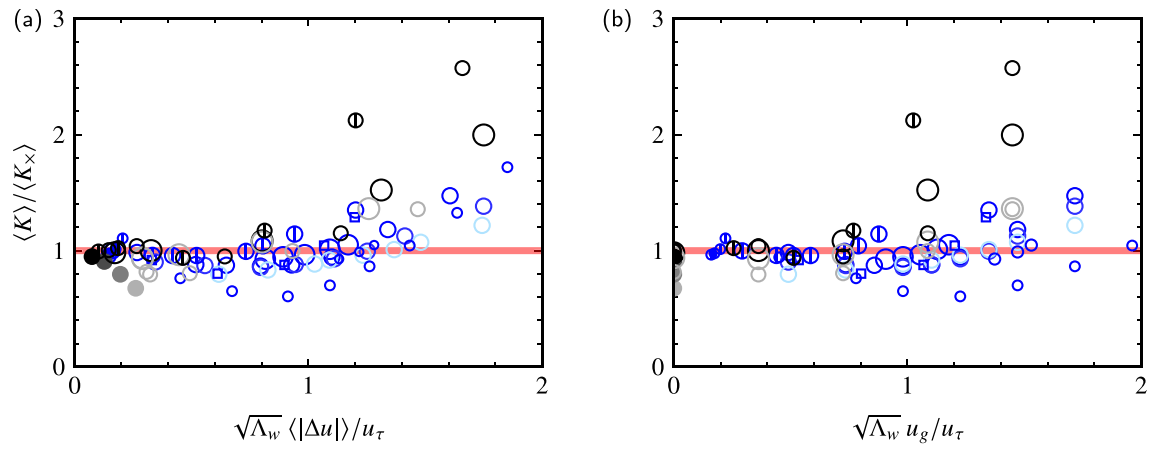

Fig. 7. Ratio of the spatial average of turbulent kinetic energy $\langle K\rangle$ to that $\langle K_x\rangle$ for the single-phase flow as functions of the indicators for turbulence enhancement, (a) $\sqrt{\Lambda_w}\langle|\Delta u|\rangle/u_\tau$ and (b) $\sqrt{\Lambda_w}u_g/u_\tau$, with assuming $\Lambda_w = 4\Lambda_p$. The open circles with a grey line show the results of the present DNS for $D/h = 0.18$ (smaller circles) and 0.36 (larger ones), and $\rho_p/\rho_f = 2$ (black) and 128 (grey). The circles with the vertical line show the results for $\Lambda_p = 0.0041$. The closed (grey) symbols show the results in Motoori and Goto (2025) at $Re_\tau = 180$. Symbols with cold colours symbols show the results for in Yu et al. (2021) in Tables 6 and 7. For the results of Motoori and Goto (2025) and Yu et al. (2021), the size and colour of the symbols indicate D/h (smaller ones indicate smaller particles) and ρ_p/ρ_f (lighter ones indicate heavier particles), respectively, and the circles with the vertical line show the results of Yu et al. (2021) for smaller volume fraction Λ_p. The red horizontal line shows $\langle K\rangle/\langle K_x\rangle = 1$.

For further larger u_g, a significant amount of K_p is added so that the total turbulent energy K can be enhanced irrespective of the attenuation rate of K_t (see $u_g/u_\tau = 8$ in Fig. 5). Incidentally, for turbulence enhancement, a large particle Reynolds number Re_p is also necessary, which is satisfied for the large particles with diameter $D^+ \geq 32$ investigated in the present study (see Fig. 3).

In summary, for $|\Delta u| \lesssim u_g$, the additional turbulent kinetic energy K_p ($\propto |\Delta u|^2$) into the wakes is not enough to enhance the total turbulent energy; whereas K_t can be attenuated due to the large energy dissipation rate ϵ_p ($\propto |\Delta u|^3/D$) around particles. In contrast, when u_g is large enough to satisfy (5), the additional K_p can lead to turbulence enhancement. Similarly to Fig. 5, we can also observe these behaviours for the spatial average turbulent kinetic energy $\langle K\rangle$; see Fig. 6, which shows the ratio of $\langle K\rangle$ to the value $\langle K_x\rangle$ in the single-phase flow as a function of u_g/u_τ. The smaller black symbols show the same parameter as in Fig. 5; namely, the result for $D/h = 0.18$ and $\rho_p/\rho_f = 2$. We can confirm that $\langle K\rangle$ is attenuated for $2 \lesssim u_g/u_\tau \lesssim 4$; whereas it gets enhanced for larger $u_g/u_\tau \gtrsim 4$. We also observe similar behaviours for heavier particles (grey circles) with larger St_h (and therefore, larger ϵ_p). Incidentally, for the larger D/h (= 0.36) (see larger circles), we can also confirm turbulence enhancement for $u_g/u_\tau \gtrsim 4$, although turbulence attenuation does not occur for $u_g/u_\tau \lesssim 4$ because of small ϵ_p. In the next subsection, to verify the sufficient condition (5) for turbulence enhancement, we use not only the present DNS results but also those by Yu et al. (2021) and Motoori and Goto (2025).

4.4. Indicator for turbulence enhancement

Fig. 7(a) shows $\langle K\rangle/\langle K_x\rangle$ as a function of the indicator $\sqrt{\Lambda_w}\,\langle|\Delta u|\rangle/u_\tau$ for turbulence enhancement, which corresponds to the right-hand side of (5) using the spatial average of the relative velocity $\langle|\Delta u|\rangle$ over y and the friction velocity u_τ. Here, we have neglected the dependence of the volume of the wake region on Re_p by assuming that it is four times larger than the particle volume (i.e. $\Lambda_w = 4\Lambda_p$). The grey open circles in the figure are the same as in Fig. 6 and those with the vertical line are the results for $\Lambda_p = 0.0041$. Symbols with cold colours show all the results (59 parameters) listed in Tables 6 and 7 of Yu et al. (2021), who conducted DNS of turbulent channel flow changing the particle diameter, mass density, settling velocity of a particle,[5] particle volume fraction and turbulence Reynolds number. Moreover, closed grey symbols show results for our previous DNS (Motoori and Goto, 2025) at $Re_\tau = 180$ under zero gravity with small ($D/h \lesssim 0.1$) particles in a wide range of the Stokes numbers ($St_h \approx 0.05$–50). It is the most important to observe that turbulence attenuation does not occur for $\sqrt{\Lambda_w}\,\langle|\Delta u|\rangle/u_\tau \gtrsim 1$ irrespective of the particle properties. In other words, for this regime, turbulence is enhanced. We can therefore conclude that (5) is a sufficient condition for turbulence enhancement.

It is also worth noting that the condition (5) can be satisfied only in the presence of gravity, where the relative velocity is approximately determined by the settling velocity u_g. In Fig. 7(b), we use u_g as the relative velocity in the horizontal axis (5), plotting the same quantity $\langle K\rangle/\langle K_x\rangle$ as in (a). The overall trend is similar to that shown in (a), although turbulence attenuation occurs even in cases satisfying $\sqrt{\Lambda_w}u_g/u_\tau > 1$. This suggests that (5) using the spatial average relative velocity (shown in Fig. 7a) gives a more accurate condition.

5. Conclusions

In the present article, we have described the physical mechanism of turbulence modulation (Section 2), and proposed the sufficient condition (5) for turbulence enhancement. When the relative velocity $|\Delta u|$ is large enough to satisfy (5), a significant turbulent kinetic energy K_p is locally introduced by the particle wakes (Fig. 2), leading to the enhancement of total turbulent kinetic energy (Fig. 7). This condition (5) cannot hold in the absence of gravity (see Section 2, and Figs. 3 and 4).

Before closing this article, we emphasise again that the relative velocity $|\Delta u|$ plays an important role in both turbulence enhancement and attenuation. As described in Section 2, the total turbulent kinetic energy K averaged in the system is expressed as the summation (1) of K_t, which is generated by external forces and/or the mean flow

layers. Therefore, the local relative velocity compared with the fluctuation velocity is larger in the outer layer (specifically, $\Delta u \gtrsim \alpha u'_x$ holds for $y/h \gtrsim 0.3$ if $\alpha = 4$). This implies that the condition (5) for turbulence enhancement can be locally satisfied from the outer layer.

[5] The directions of the settling and flow are different, which is different from ours.

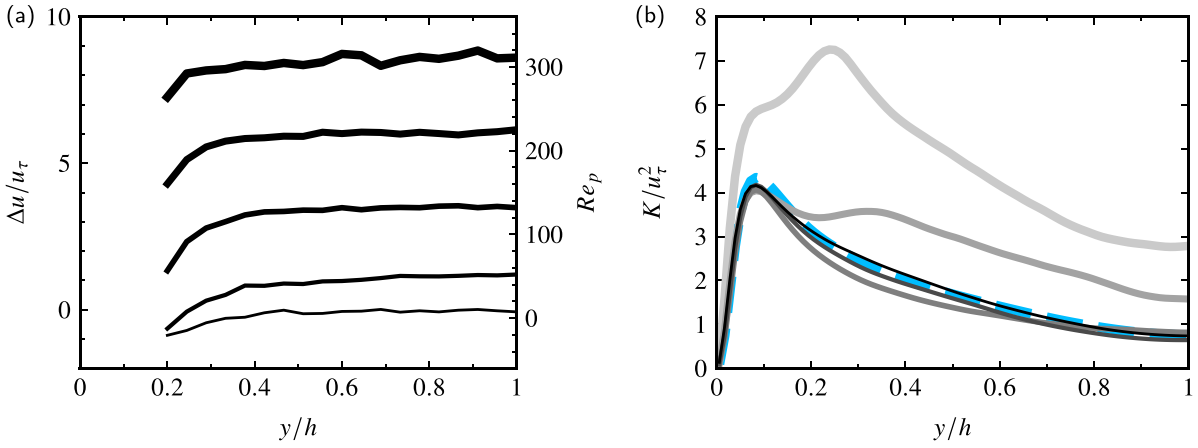

Fig. 8. Wall-normal profiles of (a) the mean streamwise relative velocity Δu and (b) turbulent kinetic energy K for $D/h = 0.18$ and $\rho_p/\rho_f = 2$ in the upward channel flow. The five lines show, from thinner [and darker in (b)] to thicker [and lighter in (b)], $u_g/u_\tau = 0$, 2, 4, 6 and 8.

without particle interactions, and K_p, which is added by the particle wakes. Note that K_t is a decreasing function of the relative velocity $|\Delta u|$, while K_p is an increasing function. A large $|\Delta u|$ leads to the additional energy dissipation in the particle wakes, which reduces the energy transfer to the energy-containing vortices, thereby attenuating K_t. In contrast, turbulence enhancement occurs when a large $|\Delta u|$ also results in a significant turbulent energy K_p being added by the particle wakes. Therefore, to predict the degree of turbulence modulation, it is necessary to estimate both the attenuation rate of K_t and the enhancement of K_p on the basis of these different roles of the particle wakes. In the present study, we have focused on the enhancement of K_p by assuming that K_t is negligible in (4). If we take into account the attenuation of K_t[6] and the dependence of Λ_w on Re_p, we can predict the degree of total turbulence modulation rate. This is left for a near future study.

CRediT authorship contribution statement

Yutaro Motoori: Writing – original draft, Investigation, Funding acquisition, Formal analysis, Data curation, Conceptualization. **Susumu Goto:** Supervision, Project administration.

Declaration of competing interest

The authors declare that they have no known competing financial interests or personal relationships that could have appeared to influence the work reported in this paper.

Acknowledgements

This study was partly supported by the JSPS Grants-in-Aid for Scientific Research, Japan 20H02068 and 23K13253. The DNS were conducted under the auspices of the NIFS Collaboration Research Programs (NIFS24KISC007) and under the supercomputer Fugaku provided by RIKEN, Japan through the HPCI System Research projects (hp230288 and hp240278).

[6] The attenuation degree of K_t is determined by ϵ_p expressed as (3). This explains the observation in Fig. 7 that the total modulation rate of K is not determined only by $|\Delta u|$ even in the case with the same Λ_p.

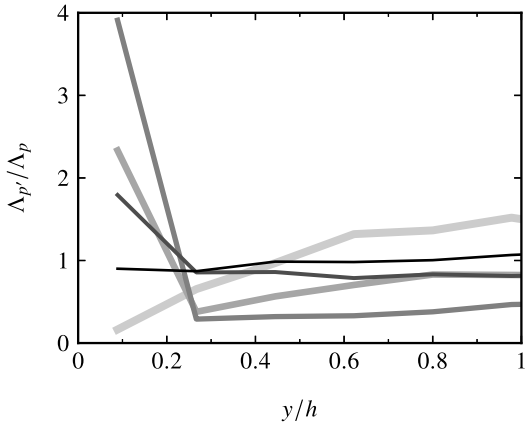

Fig. 9. Wall-normal profiles of the local particle volume fraction $\Lambda_{p'}$ normalised by the global value Λ_p for $D/h = 0.18$ and $\rho_p/\rho_f = 2$. The five lines show, from thinner and darker to thicker and lighter, $u_g/u_\tau = 0$, 2, 4, 6 and 8.

Appendix A. Upward channel flow

In this appendix, we show that the u_g-dependence of turbulence modulation is not significantly different between the downward channel flow and upward one. To demonstrate this, we conduct the DNS of upward channel flow laden with particles with $D/h = 0.18$ and $\rho_p/\rho_f = 2$, varying the settling velocity (10) of particles due to gravity: namely, $u_g/u_\tau = 2$, 4, 6 and 8. Fig. 8 shows the wall-normal profiles of (a) the mean streamwise relative velocity Δu ($= \overline{u_p - \langle u \rangle_p}$) and (b) turbulent kinetic energy K. We observe that tendencies of Δu and K with respect to u_g are similar to those observed in the downward case (see Figs. 3 and 5). More specifically, the relative velocity Δu increases monotonically with u_g, while the turbulent kinetic energy K varies non-monotonically. As u_g increases from 0, K is first attenuated; but as u_g further increases, K gets enhanced.

Appendix B. Particle concentration profile

We show in Fig. 9 the wall-normal profiles of the local particle volume fraction $\Lambda_{p'}$ normalised by the global value Λ_p. The five lines show the results for $u_g/u_\tau = 0$, 2, 4, 6 and 8. Particles distribute almost homogeneously except at $y = 0.09$ h (i.e. $y = D/2$) in the case with moderate u_g. However, the degree of accumulation is much weaker than that typically observed for small pointwise particles (Soldati and Marchioli, 2009; Bernardini, 2014; Motoori et al., 2022), and is weak

enough to explain turbulence modulation in the present study without explicitly considering the particle concentration profiles.

Data availability

Data will be made available on request.

References

Abdelsamie, A.H., Lee, C., 2012. Decaying versus stationary turbulence in particle-laden isotropic turbulence: Turbulence modulation mechanism. Phys. Fluids 24, 015106.

Balachandar, S., 2009. A scaling analysis for point-particle approaches to turbulent multiphase flows. Int. J. Multiph. Flow 35, 801–810.

Balachandar, S., Peng, C., Wang, L.P., 2024. Turbulence modulation by suspended finite-sized particles: Toward physics-based multiphase subgrid modeling. Phys. Rev. Fluids 9, 044304.

Bellani, G., Byron, M.L., Collignon, A.G., Meyer, C.R., Variano, E.A., 2012. Shape effects on turbulent modulation by large nearly neutrally buoyant particles. J. Fluid Mech. 712, 41–60.

Bernardini, M., 2014. Reynolds number scaling of inertial particle statistics in turbulent channel flows. J. Fluid Mech. 758 (R1).

Brandt, L., Coletti, F., 2022. Particle-laden turbulence: progress and perspectives. Annu. Rev. Fluid Mech. 54, 159–189.

Breugem, W.P., 2012. A second-order accurate immersed boundary method for fully resolved simulations of particle-laden flows. J. Comput. Phys. 231, 4469–4498.

Burton, T.M., Eaton, J.K., 2005. Fully resolved simulations of particle-turbulence interaction. J. Fluid Mech. 545, 67–111.

Chouippe, A., Kidanemariam, A.G., Derksen, J., Wachs, A., Uhlmann, M., 2023. 6 - results from particle-resolved simulations. In: Subramaniam, S., Balachandar, S. (Eds.), Modeling Approaches and Computational Methods for Particle-Laden Turbulent Flows. Academic Press. Computation and Analysis of Turbulent Flows. pp. 185–216.

Costa, P., Brandt, L., Picano, F., 2021. Near-wall turbulence modulation by small inertial particles. J. Fluid Mech. 922 (A9).

Dritselis, C.D., Vlachos, N.S., 2008. Numerical study of educed coherent structures in the near-wall region of a particle-laden channel flow. Phys. Fluids 20, 055103.

Ferrante, A., Elghobashi, S., 2003. On the physical mechanisms of two-way coupling in particle-laden isotropic turbulence. Phys. Fluids 15, 315–329.

Fessler, J.R., Eaton, J.K., 1999. Turbulence modification by particles in a backward-facing step flow. J. Fluid Mech. 394, 97–117.

Fornari, W., Formenti, A., Picano, F., Brandt, L., 2016. The effect of particle density in turbulent channel flow laden with finite size particles in semi-dilute conditions. Phys. Fluids 28, 033301.

Glowinski, R., Pan, T.W., Hesla, T.I., Joseph, D.D., Periaux, J., 2001. A fictitious domain approach to the direct numerical simulation of incompressible viscous flow past moving rigid bodies: application to particulate flow. J. Comput. Phys. 169, 363–426.

Gore, R.A., Crowe, C.T., 1989. Effect of particle size on modulating turbulent intensity. Int. J. Multiph. Flow 15, 279–285.

Hetsroni, G., 1989. Particles–turbulence interaction. Int. J. Multiph. Flow 15, 735–746.

Hosokawa, S., Tomiyama, A., 2004. Turbulence modification in gas-liquid and solid–liquid dispersed two-phase pipe flows. Int. J. Heat Fluids Flow 25, 489–498.

Kajishima, T., Takiguchi, S., Hamasaki, H., Miyake, Y., 2001. Turbulence structure of particle-laden flow in a vertical plane channel due to vortex shedding. JSME Intl. J. Ser. B 44, 526–535.

Kidanemariam, A.G., Chan-Braun, C., Doychev, T., Uhlmann, M., 2013. Direct numerical simulation of horizontal open channel flow with finite-size, heavy particles at low solid volume fraction. New J. Phys. 15, 025031.

Kulick, J.D., Fessler, J.R., Eaton, J.K., 1994. Particle response and turbulence modification in fully developed channel flow. J. Fluid Mech. 277, 109–134.

Kussin, J., Sommerfeld, M., 2002. Experimental studies on particle behaviour and turbulence modification in horizontal channel flow with different wall roughness. Exp. Fluids 33, 143–159.

Lee, S., Durst, F., 1982. On the motion of particles in turbulent duct flows. Int. J. Multiph. Flow 8, 125–146.

Lee, J., Lee, C., 2015. Modification of particle-laden near-wall turbulence: Effect of stokes number. Phys. Fluids 27.

Li, D., Luo, K., Fan, J., 2016. Modulation of turbulence by dispersed solid particles in a spatially developing flat-plate boundary layer. J. Fluid Mech. 802, 359–394.

Liu, C., Tang, S., Shen, L., Dong, Y., 2017. Characteristics of turbulence transport for momentum and heat in particle-laden turbulent vertical channel flows. Acta Mech. Sin. 33, 833–845.

Lucci, F., Ferrante, A., Elghobashi, S., 2010. Modulation of isotropic turbulence by particles of Taylor length-scale size. J. Fluid Mech. 650, 5–55.

Maeda, M., Hishida, K., Furutani, T., 1980. Velocity distributions of air-solids suspension in upward pipe flow: effect of particles on air velocity distribution. JSME Ser. B (Japanese) 46, 2313–2320.

Mena, S.E., Curtis, J.S., 2020. Experimental data for solid–liquid flows at intermediate and high stokes numbers. J. Fluid Mech. 883 (A24).

Mortimer, L.F., Njobuenwu, D.O., Fairweather, M., 2019. Near-wall dynamics of inertial particles in dilute turbulent channel flows. Phys. Fluids 31, 063302.

Motoori, Y., Goto, S., 2025. Attenuation mechanism of wall-bounded turbulence by heavy finite-size particles. J. Fluid Mech. (in press).

Motoori, Y., Wong, C., Goto, S., 2022. Role of the hierarchy of coherent structures in the transport of heavy small particles in turbulent channel flow. J. Fluid Mech. 942 (A3).

Muramulla, P., Tyagi, A., Goswami, P.S., Kumaran, V., 2020. Disruption of turbulence due to particle loading in a dilute gas-particle suspension. J. Fluid Mech. 889 (A28).

Oka, S., Goto, S., 2022. Attenuation of turbulence in a periodic cube by finite-size spherical solid particles. J. Fluid Mech. 949 (A45).

Peng, C., Ayala, O.M., Wang, L.P., 2019. A direct numerical investigation of two-way interactions in a particle-laden turbulent channelÂ flow. J. Fluid Mech. 875, 1096–1144.

Peng, C., Sun, Q., Wang, L.P., 2023. Parameterization of turbulence modulation by finite-size solid particles in forced homogeneous isotropic turbulence. J. Fluid Mech. 963 (A6).

Righetti, M., Romano, G.P., 2004. Particle-fluid interactions in a plane near-wall turbulent flow. J. Fluid Mech. 505, 93–121.

Rogers, C.B., Eaton, J.K., 1991. The effect of small particles on fluid turbulence in a flat-plate, turbulent boundary layer in air. Phys. Fluids A 3, 928–937.

Schneiders, L., Meinke, M., Schröder, W., 2017. Direct particle-fluid simulation of Kolmogorov-length-scale size particles in decaying isotropic turbulence. J. Fluid Mech. 819, 188–227.

Serizawa, A., Kataoka, I., Michiyoshi, I., 1975. Turbulence structure of air–water bubbly flow–III. Transport properties. Int. J. Multiph. Flow 2, 247–259.

Shen, J., Peng, C., Lu, Z., Wang, L.P., 2024. The influence of particle density and diameter on the interactions between the finite-size particles and the turbulent channel flow. Int. J. Multiph. Flow 170, 104659.

Shen, J., Peng, C., Wu, J., Chong, K.L., Lu, Z., Wang, L.P., 2022. Turbulence modulation by finite-size particles of different diameters and particle–fluid density ratios in homogeneous isotropic turbulence. 23, pp. 433–453.

Shokri, R., Ghaemi, S., Nobes, D., Sanders, R., 2017. Investigation of particle-laden turbulent pipe flow at high-reynolds-number using particle image/tracking velocimetry (piv/ptv). Int. J. Multiph. Flow 89, 136–149.

Soldati, A., Marchioli, C., 2009. Physics and modelling of turbulent particle deposition and entrainment: Review of a systematic study. Int. J. Multiph. Flow 35, 827–839.

Subramaniam, S., Balachandar, S., 2023. Modeling Approaches and Computational Methods for Particle-Laden Turbulent Flows. Academic Press.

Tanaka, T., Eaton, J.K., 2008. Classification of turbulence modification by dispersed spheres using a novel dimensionless number. Phys. Rev. Lett. 101, 114502.

Ten Cate, A., Derksen, J.J., Portela, L.M., Van den Akker, H.E., 2004. Fully resolved simulations of colliding monodisperse spheres in forced isotropic turbulence. J. Fluid Mech. 519, 233–271.

Theofanous, T., Sullivan, J., 1982. Turbulence in two-phase dispersed flows. J. Fluid Mech. 116, 343–362.

Tsuji, Y., Morikawa, Y., Shiomi, H., 1984. LDV measurements of an air-solid two-phase flow in a vertical pipe. J. Fluid Mech. 139, 417–434.

Uhlmann, M., 2005. An immersed boundary method with direct forcing for the simulation of particulate flows. J. Comput. Phys. 209, 448–476.

Uhlmann, M., 2008. Interface-resolved direct numerical simulation of vertical particulate channel flow in the turbulent regime. Phys. Fluids 20, 053305.

Uhlmann, M., Chouippe, A., 2017. Clustering and preferential concentration of finite-size particles in forced homogeneous-isotropic turbulence. J. Fluid Mech. 812, 991–1023.

Vreman, A.W., 2007. Turbulence characteristics of particle-laden pipe flow. J. Fluid Mech. 584, 235–279.

Wang, L.P., Ayala, O., Gao, H., Andersen, C., Mathews, K.L., 2014. Study of forced turbulence and its modulation by finite-size solid particles using the lattice Boltzmann approach. Comput. Math. Applics 67, 363–380.

Xia, Y., Lin, Z., Pan, D., Yu, Z., 2021. Turbulence modulation by finite-size heavy particles in a downward turbulent channel flow. Phys. Fluids 33, 063321.

Yang, T.S., Shy, S.S., 2005. Two-way interaction between solid particles and homogeneous air turbulence: Particle settling rate and turbulence modification measurements. J. Fluid Mech. 526, 171–216.

Yeo, K., Dong, S., Climent, E., Maxey, M.R., 2010. Modulation of homogeneous turbulence seeded with finite size bubbles or particles. Int. J. Multiph. Flow 36, 221–233.

Yu, Z., Lin, Z., Shao, X., Wang, L.P., 2017. Effects of particle-fluid density ratio on the interactions between the turbulent channel flow and finite-size particles. Phys. Rev. E 96.

Yu, Z., Xia, Y., Guo, Y., Lin, J., 2021. Modulation of turbulence intensity by heavy finite-size particles in upward channel flow. J. Fluid Mech. 913 (A3).

Zhao, L.H., Andersson, H.I., Gillissen, J.J., 2010. Turbulence modulation and drag reduction by spherical particles. Phys. Fluids 22, 081702.

Zhao, L., Andersson, H.I., Gillissen, J.J., 2013. Interphasial energy transfer and particle dissipation in particle-laden wall turbulence. J. Fluid Mech. 715, 32–59.